CrossMark

Flame-Flow Interaction in Premixed Turbulent Flames During Transient Head-On Quenching

Martin Rißmann[1] (ORCID) **· Christopher Jainski[1] ·
Markus Mann[1] · Andreas Dreizler[1]**

Abstract This paper reports on experimental investigations of turbulent flame-wall inter-action (FWI) during transient head-on quenching (HOQ) of premixed flames. The entire process, including flame-wall approach and flame quenching, was analyzed using high rep-etition rate particle image velocimetry (PIV) and simultaneous flame front tracking based on laser-induced fluorescence (LIF) of the OH molecule. The influence of convection upon flame structures and flow fields was analyzed qualitatively and quantitatively for the fuels methane (CH_4) and ethylene (C_2H_4) at $\phi = 1$. For this transient FWI, flames were initial-ized by laser spark ignition 5 mm above the burner nozzle. Subsequently, flames propagated against a steel wall, located 32 mm above the burner nozzle, where they were eventually quenched in the HOQ regime due to enthalpy losses. Twenty ignition events were recorded and analyzed for each fuel. Quenching distances were 179 μm for CH_4 and 159 μm for C_2H_4, which lead by nondimensionalization with flame thickness to Peclet numbers of 3.1 and 5.5, respectively. Flame wrinkling and fresh gas velocity fluctuations proved flame and flow laminarization during wall approach. Velocity fluctuations cause flame wrinkling, which is higher for CH_4 than C_2H_4 despite lower velocity fluctuations. Lewis number effects explained this phenomenon. Results from flame propagation showed that convection dominates propagation far from the wall and differences in flame propagation are related to the different laminar flame speeds of the fuels. Close to the wall flames of both fuels

✉ Martin Rißmann
  rissmann@rsm.tu-darmstadt.de

  Christopher Jainski
  jainski@rsm.tu-darmstadt.de

  Markus Mann
  markus.mann@sandvik.com

  Andreas Dreizler
  dreizler@rsm.tu-darmstadt.de

[1] Institute of Reactive Flows and Diagnostics (RSM), Technische Universität Darmstadt,
    Jovanka-Bontschits-Straße 2, 64289 Darmstadt, Germany

propagate similarly, but experimental results clearly indicate a decrease in intrinsic flame speed. In general, the experimental results are in good agreement with other experimental studies and several numerical studies, which are mainly based on direct numerical simulations.

Keywords Flame-wall interaction · Quenching · Turbulent · Premixed · Laser diagnostics

1 Introduction

The development of modern combustion devices such as IC engines and gas turbines is towards higher power densities and therefore smaller surface area to volume ratios. Thus, flame-wall interaction (FWI) is of increasing importance in this context. Combustor walls are exposed to extremely high temperatures which eventually leads to fatigue failure of the material. However, combustor walls are cooled causing enthalpy loss in the combustion process. This leads to reduced efficiency and incomplete combustion which results in the formation of pollutants, e.g. CO [1, 2].

FWI strongly couples processes of flow field, flame chemistry and wall properties [3]. Flames close to a wall get quenched eventually due to enthalpy losses. FWI generally has two canonical configurations: Side-wall quenching is defined by wallparallel flame propagation; the configuration investigated in this work, head-on quenching (HOQ), is characterized by wallnormal flame propagation.

This study focuses on transient turbulent FWI of premixed flames in the HOQ configuration. The impact of a convective flow field and fuel type on FWI is investigated as it is particularly relevant in IC engines, where the flame partly impinges orthogonally on enclosing walls.

Laminar premixed flames in transient FWI of HOQ used to be investigated using simple fuels, such as CH_4. Reference [4] experimentally analyzes flame structures and velocities in laminar HOQ; however the fresh gases are initially quiescent different to the flow of this study. References [5–7] use the same burner as in the present study to experimentally characterize thermokinetics, heat transfer and flame structures during HOQ. In these studies the flame is ignited in a laminar convective flow field. Numerical simulations are usually limited to 1-D calculations with simplified chemistry, e.g. [8, 9], or are a part of turbulent HOQ studies, e.g. [10, 11]. References [9, 12, 13] use detailed chemistry of different fuels in 1-D simulations of laminar HOQ, focusing on species' concentrations, heat flux and wall temperature. Reference [13] focuses on quenching and pressure influence for various fuels.

Few studies on turbulent premixed flames in transient HOQ exist. References [14–16] use a constant volume vessel to experimentally investigate velocities and heat flux during FWI of a premixed CH_4 flame. The fresh gases are initially in a tumble motion. Using simulations, ref. [10] applies 2-D DNS to analyze quenching distances, flame propagation and heat flux during transient HOQ of a premixed flame in a synthetic turbulent flow field. Reference [11] studies the effect of different Lewis numbers on quenching distances and turbulent flame lengths during transient turbulent HOQ with the aid of 2-D DNS. Reference [17] uses a 3-D DNS in a channel flow to focus on flame-flow interaction during HOQ. In general, these 2-D and 3-D DNSs are all based on simplified chemistry and synthetic turbulence.

This work has two major objectives: to analyze the impact of a turbulent convective flow field and to investigate the influence of various fuels on transient HOQ of premixed turbulent flames. Neither of these objectives has yet been subject to any experimental study.

Unlike existing numerical studies this experimental work is restricted to weakly wrinkled flames but is not limited to synthetic turbulence or simplified chemistry. For the experimental investigation cinematographic stereo-PIV (to measure velocities) and planar OH-LIF (to simultaneously track flame fronts) are combined. Selected snapshots of these time-resolved measurements enable qualitative description of the transient FWI of individual quenching events. Characteristic properties of turbulent flames in the context of FWI, such as turbulent flame length, fresh gas velocity fluctuations and flame propagation are quantified.

2 Experiment Set-Up

2.1 Burner configuration

Transient, premixed turbulent flame-wall interaction in the head-on quenching regime is realized using a nozzle type burner (Fig. 1). A laser spark at the nozzle exit, $r = 0$ mm, $z = 27$ mm, ignites premixed air and fuel (refer to [6] for more details). A flame then propagates orthogonally against a steel wall, where it eventually gets quenched due to the enthalpy losses. The water-cooled wall is spherical-shaped ($R = 300$ mm) and located at
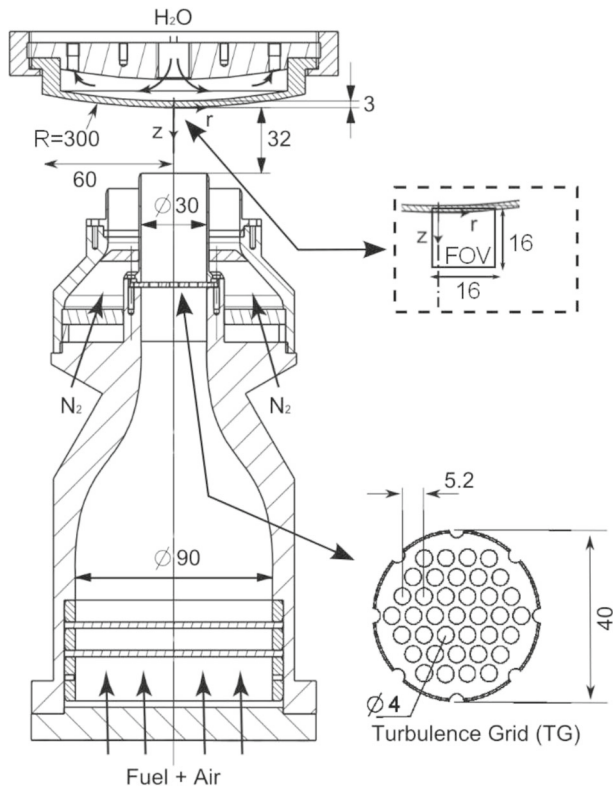

Fig. 1 Sketch of the FWI impinging jet burner with turbulence grid. Dimensions are given in mm. For further details see text and refer to [5–7, 18]. The field of view (FOV) for the PIV and OH measurement in the central plane of the burner and the coordinate system are illustrated in the *dashed box*

$z = 0$ mm at a distance of 32 mm from the nozzle exit. The burner used in this study is the same as that used in ref. [5–7, 18]. Figure 1 details the burner including the turbulence grid (TG) used. The TG enhances the turbulence level to $\frac{u'}{u} \approx 6-7\%$ (u is the bulk flow velocity and u' is the axial velocity fluctuations at the nozzle exit). The integral length scale at the nozzle exit equals $l_{int} \approx 4.7$ mm (data taken from ref. [6]). All gas flows are controlled by electronic mass flow meters (Bronkhorst EL-Flow series). Fuel, methane (CH_4) or ethylene (C_2H_4), and air are mixed well and fed into the burner at room temperature and atmospheric pressure. Fine meshes in the lower section of the burner homogenize the flow. The premixed jet exits the burner with a bulk flow velocity of approximately 2.62m/s. This corresponds to a Reynolds number of $Re = 5000$ based on the fluid properties of the unburnt mixture at 273 K, 1 atm and the nozzle exit diameter of $d = 30$ mm. A nitrogen coflow with a bulk flow velocity of approximately 1.31 m/s (50 % of the jet velocity) surrounds the premixed jet to shield it from external influences. Operating conditions and relevant parameters are summarized in Table 1. Based on estimations of $\frac{u'}{s_l} < 1$ and $\frac{l_{int}}{\delta_{flame}} = 82(CH4), 162(C2H4)$, premixed flames of both fuels are located in the wrinkled regime as in ref. [19]. The origin of a Cartesian coordinate system (detail of Fig. 1) is defined at the stagnation point of the jet in the measurement plane. The central axis z is aligned with the nozzle's main axis; the radial axis r is perpendicular to z and the tangential coordinate t points into the plane of Fig. 1.

2.2 Combined OH-PLIF and PIV

Flame-wall interaction is characterized cinematographically at 10 kHz recording rate using stereoscopic PIV to measure velocities and simultaneous planar OH-LIF to track flame fronts. These techniques are applied simultaneously in the central plane of the nozzle (Fig. 1). For PIV measurements the premixed jet flow is seeded with Al_2O_3 particles (Ø1 μ m) and illuminated by a frequency-doubled Nd:YVO$_4$ laser ($\lambda = 532$ nm, 4.0 mJ/pulse, pulse separation 100 μs, Edgewave IS 4II-DE) at 10 kHz repetition rate. OH fluorescence is excited at the Q$_1$(6)-transition ($\lambda = 282.93$ nm, 0.25 mJ/pulse) using a frequency doubled high-speed dye laser (Sirah Credo, Rhodamine 6G) pumped at 10 kHz by an Nd:YAG laser ($\lambda = 532$ nm, 8 mJ/pulse, Edgewave CX 16II-E). Laser beams are formed into ~100 μm thick light sheets and are combined into one imaging plane using a dichroic mirror (high-reflective at $\lambda = 283$ nm, high-transmissive at $\lambda = 532$ nm). The dye laser is fired in between the PIV laser pulses. For stereoscopic PIV the Mie-scattering of Al_2O_3 particles is imaged with 180 mm f/3.5 macro lenses and Scheimpflug adapters on high-speed CMOS cameras (LaVision HSS 6). Both PIV cameras have a field of view (FOV) of 17×17 mm^2 and are arranged symmetrically to the laser light sheets with an angle

Table 1 Operating conditions for transient flame-wall interaction

fuel	ϕ	$s_l[m/s]$	u'/s_l [−]	$\delta_{flame}[\mu m]$	$Le[-]$
CH_4	1	0.38	0.48	57.1	1.01
C_2H_4	1	0.68	0.27	29.0	≈ 1.2

ϕ is the equivalence ratio, s_l is the undisturbed laminar flame speed, taken from [20], u'/s_l is the ratio of the axial velocity fluctuations at the nozzle exit (data from [6]) over the undisturbed laminar flame speed, $\delta_{flame} = \frac{\lambda}{\rho C_p s_l}$ is the flame thickness based on the mixture in [21]. For C_2H_4 the Lewis number is from [22] and for C_2H_4 the value is taken for a similar mixture from [23]

of ∼30°. OH-LIF signals are imaged with a 150 mm UV lens (Halle OUC 3.60.4) on an image intensifier (LaVision HighSpeed IRO) coupled to another CMOS camera (LaVision HSS 5). This camera system, with a FOV of 16×16 mm^2, is arranged perpendicularly to the laser light sheet plane.

The PIV data are calibrated using a stereoscopic PIV target and the OH data are calibrated using a 1 mm grid target. The two systems are matched based on images of the 1 mm grid target.

LaVision Davis PIV software is used to post-process the PIV data. Adaptive interrogation windows 24×24 pixels in size and with 75 % overlap are used to calculate the velocity fields, resulting in a vector spacing of 144 µm. Outliers are filtered with a 3x3 median filter. Flame front positions are extracted from the instantaneous OH images. The noise in the images is reduced using a non-linear diffusion filter, as suggested by [24] for application in turbulent flames and successfully applied by [5] to laminar flames in the same head-on quenching configuration as this paper. This filter, originally developed by [25], preserves and enhances the OH gradients while removing noise. The filtered OH image is then interpolated cubically by a factor of 4 to avoid any jumps in detection of the flame front. In the final step the flame front is extracted from the filtered images by detecting the steepest OH gradient with a Canny-Edge filter [26] in Matlab.

2.3 Data-acquisition, wall position and measurement uncertainties

For each operational condition of Table 1, 20 ignition events are realized. Each event is recorded as a sequence of 200 images, which is a recording length of 20 ms and is a compromise between necessary samples for statistical data evaluation and the complexity of the experimental procedure. All events cannot be considered for some evaluated parameters, since flame front detection sometimes fails due to laser and signal intensity fluctuations. This is especially the case for CH_4 flames, as they generally have a lower signal-to-noise ratio of the OH-LIF than C_2H_4 flames.

The exact wall position is determined from the average intensity of the 200 PIV raw images per ignition event. In the average image, the reflections from the wall due to the laser light are clearly visible. A circle with radius $R = 300$ mm matching the shape of the curved wall is fitted to the reflections. The wall position is then obtained. In the final step the ensemble average of the determined wall positions is calculated for each fuel. The systematic error of this procedure corresponds to the standard deviation of the determined wall position, which is 160 µm in the radial direction r and 5 µm in the wall normal direction z.

As mentioned previously, the PIV and the OH systems are matched using a grid target with 1 mm line spacing. The OH image resolution is the limiting factor. Based on line thickness of the target the resolution is estimated as being 65 % inferior to that of the PIV image. The systematic matching error is estimated to be 82 µm based on the line positions. This is assumed as the dominant error source of this measurement compared to other possible uncertainties (e.g. time and spatial resolution).

2.4 Determination of quenching and spatial representation

Flame quenching is determined from the OH images based on the OH gradient. During wall approach, the OH gradient in vertical direction z is tracked for each flame element. When the flame senses the wall, the OH gradient decreases until it vanishes entirely. The instant of quenching is defined as being where the OH gradient, normalized to its maximum value far-off the wall, falls below 0.5. In ref. [27], this approach is successfully applied to side-wall

quenching flames and validated by comparison to chemoluminescence imaging. Thus the quenching distance δ_{quench} corresponds to the location z of this event corrected for the wall position at the specific radial location r. This correction is necessary due to the curvature of the wall (Fig. 1).

When analyzing the characteristic processes of transient FWI, spatial representation depending on the distance between the flame and the wall can suppress intermittence effects observed in a laboratory-fixed representation of turbulent flames. To achieve this, the instantaneous axial flame front position is sorted into radial Δr and wall normal Δz bins (Fig. 2). First, Fig. 2a, each instantaneous flame front is divided radially into bins of $\Delta r = 500$ µm. Next, in each bin, the wall normal flame position is corrected for the wall position and a mean flame position z_{FF} is calculated. The spatial representation is obtained by sorting z_{FF} and flame properties, such as the turbulent flame length L_t at this position into wall normal bins of $\Delta z = 500$ µm (Fig. 2b). This method has the drawback that in the case of highly wrinkled flames z_{FF} is the average position of several flame elements in one radial bin Δr (compare Fig. 2a $6.5mm < r < 8$ mm). However, this is only observed occasionally for CH_4 flames. Far off the wall, $z > 4$ mm, 5 out of 20 CH_4 ignition events exhibit this phenomena in certain radial bins Δr. At maximum only 4 % of all Δr per instantaneous flame front are concerned. Close to the wall, $z < 4$ mm, this phenomena does not occur any more. Further consequences are discussed for L_t in Section 3.3.

The influence of the bin widths (Δr and Δz) on the behaviour of the quantities evaluated in this study has been analyzed and results (not shown) show similar behaviour independent of the size of Δ. Quenched flame elements are not considered in the statistical evaluation.

3 Results

3.1 Flame evolution

Transient FWI, leading to head-on quenching is discussed qualitatively in this section, based on Fig. 3. Instantaneous snapshots including the evolution of the flame front and the absolute velocity field $|u| = \sqrt{u_{axial}^2 + u_{radial}^2 + u_{tangential}^2}$ of a single ignition event of CH_4 a) and
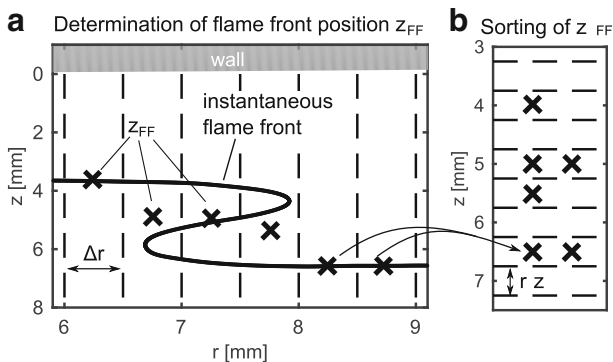

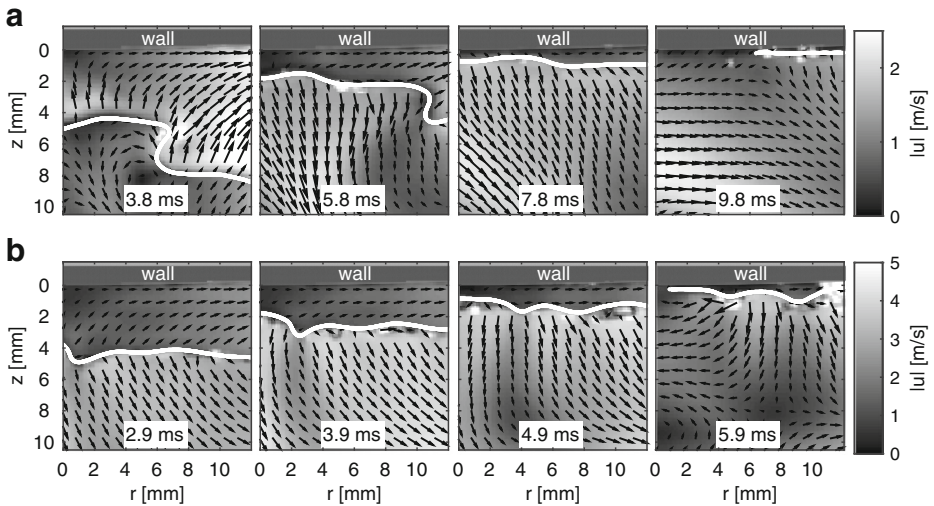**Fig. 2** Post-processing steps for spatial representation of FWI parameters, depending on the flame-wall distance

Fig. 3 Flame front (*white line*) and velocity field for CH$_4$ (**a**) and C$_2$H$_4$ (**b**) at different time steps for a single quenching event. $\tau = 0$ ms at ignition

C$_2$H$_4$ b), are shown. Overall, the FWI process of the C$_2$H$_4$ flame is considerably faster than the CH$_4$ flame because of the higher flame speed (Table 1).

Regarding the velocity in the r-z-plane, the acceleration of the burnt gases is up to twice the absolute velocity of the fresh gases and the turnover of the vectors in the wall normal direction is due to the passage of the flame. The flame passage disturbs the typical stagnation point flow, with high radial velocities for $|r| \gg 0$ mm.

In flame front evolution, the impact of the wall is obvious since the turbulent flame fronts are laminarized during wall approach, which confirms the DNS observations of [10] and [11]. Additionally, Fig. 3 reveals that at times $\tau = 9.8$ ms for CH$_4$ a) and $\tau = 5.9$ ms for C$_2$H$_4$ b) quenching does not occur homogenously along the wall surface. It starts at particular points, corresponding usually to convex flame elements (not shown), and then propagates parallel to the wall until the whole flame is quenched entirely. This general experimental observation is in full agreement with the DNS-based explanations of [10]. Concave flame elements, e.g. Fig. 3b at $\tau = 5.9$ ms remain relatively long at the wall, before they finally get quenched. Low flow field velocities and disturbed flame chemistry slow the consumption of the remaining gas thus causing this phenomenon. The CH$_4$ flame is clearly more sensitive to flame-flow interactions inducing strong flame front wrinkling (Fig. 3a at $\tau = 3.8$ and 5.8 ms). This can be related to the different Lewis numbers of the investigated fuels. For $Le > 1$ (C$_2$H$_4$) flame wrinkling due to external disturbances, such as velocity fluctuations u' / s_l, vanishes quickly, whereas it remains or is amplified for $Le \leq 1$ (CH$_4$) [11, 23, 28, 29].

3.2 Quenching distances

An initial characteristic measure of flame quenching at a wall is the quenching distance δ_{quench}. Non dimensionalizing δ_{quench} by the flame thickness δ_{flame} (Table 1) leads to the quenching Peclet number Pe. Table 2 summarizes the results obtained. The standard

Table 2 Mean quenching distances evaluated between r = [0–12] mm

Fuel	Considered ignition events	$\delta_{quench}[\mu m]$	Pe [-]
CH_4	15/20	179 ± 56	3.1 ± 1
C_2H_4	18/20	159 ± 34	5.5 ± 1.2

Failures in flame front detection due to weak OH gradients near the wall cause negation of certain ignition events for this evaluation

deviation of δ_{quench} and Pe is related to the turbulent nature of the FWI. Systematic errors are estimated and discussed in Section 2.3

Reference [6] measured $\delta_{quench} = 170$ μm for CH$_4$ based on a temperature criterion on the same burner at otherwise identical operational conditions except for the laminar flow conditions. According to [10, 11] δ_{quench} of turbulent and laminar flames is similar. This is the case for the turbulent CH$_4$ flame of this study with $\delta_{quench} = 179$ μm

Peclet numbers Pe are in an expected range for head-on quenching [3]. However values for the two fuels are different, which contrasts to ref. [3, 13], who state that Pe is independent of the fuel type for hydrocarbons. Based on DNS [11] states that smaller Lewis numbers lead to higher Peclet numbers. This was not observed in the experimental data of this work, which might be due to the different flame regime investigated here.

3.3 Flame length

Turbulent flame front length L_t is an appropriate way to quantify laminarization of the flame front during wall approach (Fig. 3). L_t is defined here as the length of each flame element in a radial bin Δr (compare Fig. 2a). The obtained L_t are sorted according to the flame position z_{FF}; and the mean and standard deviation of L_t in each bin Δz is calculated (compare Fig. 2b). The results are nondimensionalized by the bin width Δr, which is assumed to correspond to the unwrinkled laminar flame length L_l. As mentioned in Section 2.4 this method has some drawbacks: For L_t this means that several flame elements in one radial bin Δr contribute to L_t in the case of intense flame wrinkling (compare Fig. 2a 6.5 mm < r < 8 mm). Nevertheless, this approach clearly differentiates between laminar and turbulent flames, which is the aim of this section. The problem could be circumvented using the approach of ref. [27]: The instantaneous L_t is determined spatially in each equal-sized square of a grid. However, this approach is not feasible here, since the sample size is relatively low.

Figure 4 shows the evolution of L_t as a function of the flame position z. Depending on the fuel, different zones can be defined. For $z > 3$ mm FWI of CH$_4$ is dominated by flame-turbulence interaction, and flame wrinkling is strongly damped during wall approach (compare Fig. 4a and b). Referencing [10], this zone is called "inhibition zone". C$_2$H$_4$ does not exhibit such a zone, mainly due to the higher Lewis number, which causes the flame to be less wrinkled [11, 23, 29]. Between $1 < z < 3$ mm L_t shows similar behaviour for both fuels with almost constant L_t. However, C$_2$H$_4$ features slightly higher fluctuation levels, although they remain at the same level as for $z > 3$ mm (compare Fig. 4b). Finally, for $z < 1$ mm L_t decreases and approaches the laminar flame length L_l. Referring to [10] this zone could be considered as the transition to the "influence zone", where the flame starts sensing the wall and the quenching process is induced. Generally, the experimental
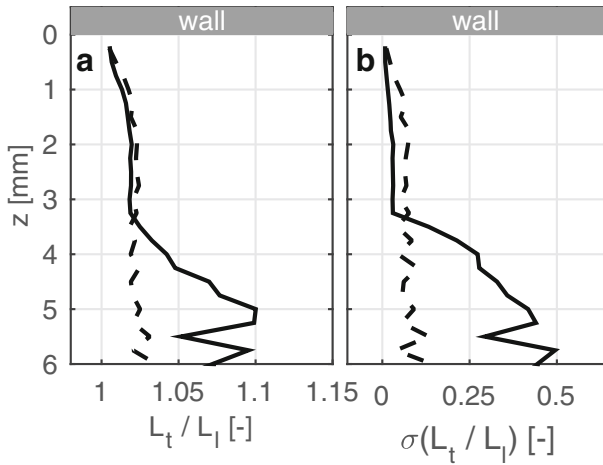
Fig. 4 Normalized flame lengths for CH_4 (-, 19/20 ignition events) and C_2H_4 (- -, 19/20 ignition events) as a function of the flame position z. **a** mean and **b** fluctuations evaluated for r ∈ [0–12] mm, with $\Delta r = \Delta z = 500 \,\mu m$

observations confirm the DNS studies of [11], which state that during FWI higher Lewis numbers lead to less flame wrinkling and in certain cases to almost constant L_t.

3.4 Fluctuations

The velocity fluctuations of the fresh gases in the direction of flame propagation are analyzed to judge the influence of flame-flow interaction on transient head-on quenching processes. First, the instantaneous flame normal vector $\vec{n}$ pointing towards the fresh gases is calculated in the r-z-plane for each flame front element in a radial bin Δr (Section 2.4 and Fig. 2). Second, the axial $\vec{u}_{axial}$ and radial $\vec{u}_{radial}$ velocity components are extracted at a distance of $\Delta n = 1$ mm ahead of the flame front to circumvent unknown density effects caused by the expanding flame [27]. The influence of Δn on the results of this section has been analyzed in a sensitivity study within a range of $\Delta n \in [0.5, 1.5]\,mm$ No major differences have been observed (not shown here). After projecting these components onto the flame normal direction $\vec{n}$, the mean velocity is calculated in each bin Δr. The sum of the obtained components $\vec{u}_{radial,n}$ and $\vec{u}_{axial,n}$ is $\vec{u}_{absolute,n}$ (Fig. 5). Next, the obtained values are sorted according to the vertical flame position z_{FF}. The standard deviation in each axial bin Δz then results in the velocity fluctuations $u'_{radial,n}$, $u'_{axial,n}$ and $u'_{absolute,n}$. Results are normalized by the laminar flame speed s_l to compare the two fuels.

Figure 6 shows components of the fresh gas velocity fluctuations in the flame normal direction. The results clearly show that the absolute turbulence level of the fresh gas decreases during wall approach (Fig. 6a). Consequently, the wall damps turbulence in the fresh gas flow. The rate of turbulence decrease in axial direction (Fig. 6b) can be considered as constant for positions of $z < 4mm$. For the radial component turbulence decrease is only observed very close to the wall (Fig. 6c $z < 1.75$ mm for CH_4 and $z < 3$ mm for C_2H_4).

While the axial component, Fig. 6b, shows similar behaviour for both fuels, the radial component Fig. 6c shows clear differences. The radial component is quite revealing since its amplitude for CH_4 is inferior to that of C_2H_4. It is well known from turbulent flame theory and experimental studies, e.g. [22], that higher turbulence causes more flame wrinkling.
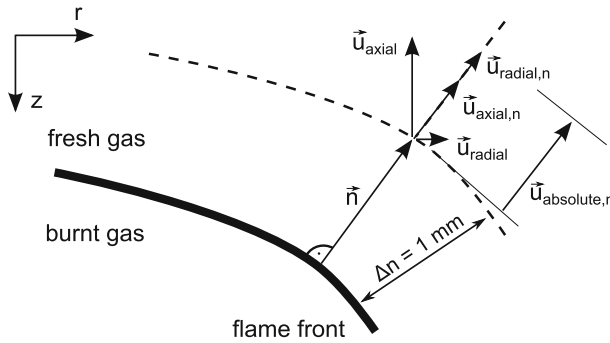
Fig. 5 Sketch of the flame normal vector $\vec{n}$ of a single flame front element and the related velocity vector components $\vec{u}_{radial,n}$ $\vec{u}_{axial,n}$ and $\vec{u}_{absolute,n}$

However, we observe the opposite for the near wall flame. When neglecting the possible influence of the processing method for L_t, one can therefore conclude that the higher wrinkling of the CH_4 flame (compare Fig. 3a and Fig. 4a) is related to Lewis number effects as discussed in Section 3.1. Hence diffusion processes are suspected to be the reasons for stronger flame wrinkling [11, 23, 28, 29].

In the case of FWI, local values of u'/s_l close to the instantaneous position of the flame rather than global values at the nozzle exit should be considered. The ratio u'/s_l is influenced by the presence of the wall and can be significantly different compared to the unbounded flow. This might be the reason for discrepancies to observations from the previous work by Renou and Boukhalfa [22]. In contrast to the present findings, a higher Lewis number caused increased flame wrinkling at a similar turbulence level to this work ($u'/s_l \approx 0.9$). At a slightly higher turbulence level ($u'/s_l \approx 1.3$), however, an increasing Lewis number decreased the flame wrinkling which appears similar to the observations of this work.

3.5 Flame propagation

Flame propagation during FWI is important, since enthalpy losses to the wall strongly disturb the combustion process [3, 6]. Calculation of the turbulent flame displacement speed
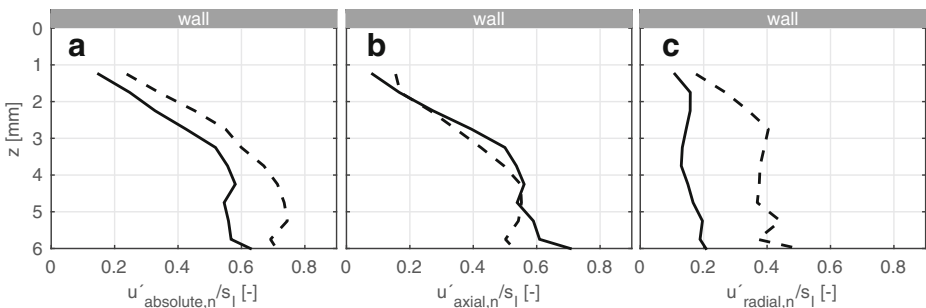

Fig. 6 Velocity fluctuations in the fresh gas in flame normal direction for CH_4 (–, 19/20 ignition events), C_2H_4 (- -, 18/20 ignition events). Values are extracted at $\Delta n = 1$ mm ahead of the flame front and evaluated for $\Delta r = \Delta z = 500$ μm, $r \in [0–12]$ mm. **a** absolute fluctuations, **b** axial component and **c** radial component

s_t, e.g. in [30], from the experimental data is not feasible because of the low sample number and the 3-dimensional flame propagation. Since only a few studies have characterized transient head-on quenching in a convective flow, the evolution of the flame front position z_{FF} as a function of time τ is a parameter of interest. Figure 7 shows the mean evolution of this parameter along the centreline of the burner at $\Delta r = [0 - 0.5]\,mm$. For each ignition event the instant of quenching at this radial position is determined and is set to $\tau = 0ms$. This allows the calculation of an ensemble average of the flame position z_{FF} as a function of time τ prior to quenching.

The results of Fig. 7 quantify and confirm the qualitative findings of Fig. 3, stating that the C_2H_4 flame reaches the wall faster than the CH_4 flame. The decreasing standard deviation of z_{FF} in Fig. 7 clearly proves the laminarization of the flame front, especially for times $\tau > -2ms$ prior to quenching. For both fuels $z_{FF}(\tau)$ has a parabolic shape with asymptotic behaviour close to the wall. The experimental results of $z_{FF}(\tau)$ for turbulent flames from this study demonstrate a similar behaviour to the findings in [7] resulting from 1-D CARS thermometry measurements of a laminar CH_4 flame at the same ϕ and conditions on the same burner. For turbulent flames the trend of the measured $z_{FF}(\tau)$ corresponds well to the DNS observations in [10] and [11].

The absolute flame speed u_{FF} in the r-z plane provides further insight into transient head-on quenching of premixed turbulent flames. The absolute flame speed u_{FF} results from the superposition of the convective velocity of the unburnt gases and the local flame displacement speed s_t [30]. Due to the relatively small sample number in this study, a time derivation of the curves in Fig. 7 would cause noisy u_{FF}. Thus, a different procedure for determining u_{FF} is used: First, the mean axial flame position z_{FF} is calculated for each instantaneous flame front in $\Delta r = [0 - 0.5]\,mm$. This leads to a function $z_{FF}(\tau)$, which is then derived in time for each ignition event. In the last step, $dz_{FF}/d\tau = u_{FF}$ is sorted according to z_{FF} and the mean is calculated in each bin Δz (Section 2.4). Normalization to the undisturbed laminar flame speed s_l allows better comparability of the two fuels. It is expected that $u_{FF} \rightarrow 0$ m/s at the wall. Due to collection into bins $\Delta z = 500\,\mu m$, this is not observable in this study.

The results for $u_{FF}(z)$ including the standard deviation are shown in Fig. 8. Previous observations on laminarization and the faster FWI process of C_2H_4 (hidden here by the normalization to s_l) are observed again. Generally, far off the wall, for z > 1 mm, flame propagation is driven primarily by the convective flow field. Additionally, u_{FF} strongly decreases at quasi-constant rates during wall approach. Since both fuels show the same normalized u_{FF} differences in the overall propagation process are related to the reactive/diffusive properties of the fuels which is expressed through the laminar flame speed s_l

Fig. 7 Flame position z_{FF} over time τ (referenced to the instant of quenching) for CH_4 (–, 17/20 ignition events) and C_2H_4 (- -, 19/20 ignition events) evaluated for r ∈ [0–0.5] mm. *Error bars* indicate the standard deviation of the flame position (for better readability only every second *error bar* is shown)
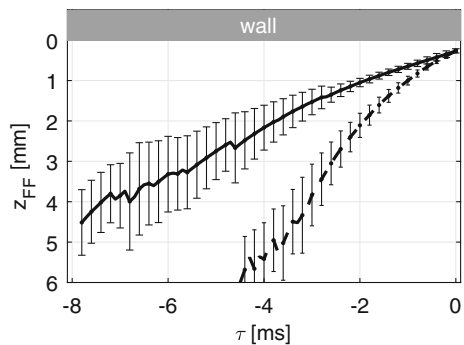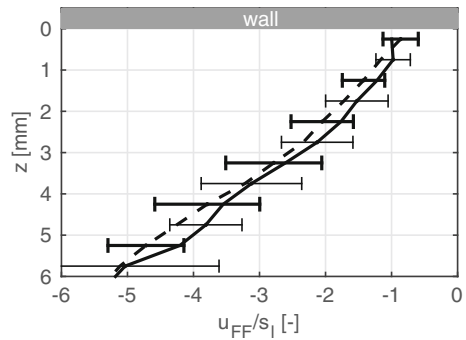
Fig. 8 Absolute flame speed u_{FF} normalized by laminar flame speed s_l, including standard deviation for CH$_4$ (–, *thin error bars*, 17/20 ignition events), C$_2$H$_4$ (- -, *thick error bars*, 19/20 ignition events) as a function of the distance to the wall. Evaluated for r ∈ [0–0.5] mm with $\Delta r = \Delta z = 500$ μm. For better readability only every second error bar is shown

(Table 1). Consequently, the influence of convection on the flame propagation of both fuels is identical.

Close to the wall, for $z < 1$ mm, both fuels exhibit $\left| u_{FF}/s_l \right| \leq 1$. This again proves the transition to the influence zone (compare to Section 3.3). This observation strongly indicates a decrease in the flame displacement speed s_t and changes in the laminar flame speed [10, 27].

Experimental quantification of u_{FF} during HOQ has not yet been published in literature. Qualitative comparison of the results with various numerical simulations shows that they are in good agreement: [8] uses 1-D simulations to calculate the absolute flame speed for a laminar premixed flame during HOQ. However, the fresh gas is initially quiescent. In turbulent premixed HOQ, the absolute flame speed could be deduced from the flame position over time as in [10] and [11].

4 Conclusion

Flame-flow interactions (FWI) during transient head-on quenching of turbulent premixed CH$_4$ and C$_2$H$_4$ flames were investigated. Qualitative observations based on selected instantaneous snapshots from the time series data of the velocity field and the flame position clearly show the different behaviour of the flame shape and the overall FWI process speed. However, both fuels show laminarization of flow and flame during wall approach. The quantitative findings of this work, such as the quenching distance δ_{quench} and the turbulent flame length L_t, are in good agreement with DNS calculations, which are restricted to simplified chemistry and synthetic turbulence and handle different flame regimes. This work is the first known quantification of fresh gas velocity fluctuations u'/s_l in the context of FWI. u'/s_l induces flame wrinkling which is expressed by L_t. The different fuels reveal that it is primarily Lewis number effects not the amplitude of the flow field fluctuations, that mainly influence L_t. Finally, flame propagation shows that convection dominates flame propagation far off the wall and differences are only related to different reactive/diffusive properties, expressed by the laminar flame speed of the fuel. Close to the wall the absolute flame speeds are inferior to the undisturbed laminar flame speeds and thus strongly indicate disturbances in the flame chemistry.

Compliance with Ethical Standards

References

1. Alkidas, A.C.: Combustion-chamber crevices: the major source of engine-out hydrocarbon emissions under fully warmed conditions. Prog. Energ. Combust. **25**, 253–273 (1999)
2. Roberts, A., Brooks, R., Shipway, P.: Internal combustion engine cold-start efficiency: a review of the problem, causes and potential solutions. Energ. Convers. Manage. **82**, 327–350 (2014)
3. Dreizler, A., Böhm, B.: Advanced laser diagnostics for an improved understanding of premixed flame-wall interactions. Proc. Combust. Inst. **35**, 37–64 (2015)
4. Foucher, F., Burnel, S., Mounaïm-Rousselle, C., Boukhalfa, M., Renou, B., Trinité, M.: Flame wall interaction: effect of stretch. Exp. Therm. Fluid Sci. **27**, 431–437 (2003)
5. Mann, M.: Laserbasierte Untersuchung Der Flamme-Wand-Interaktion. Göttingen, Optimus-Verlag (2013)
6. Mann, M., Jainski, C., Euler, M., Böhm, B., Dreizler, A.: Transient flame–wall interactions: experimental analysis using spectroscopic temperature and CO concentration measurements. Combust. Flame **161**, 2371–2386 (2014)
7. Bohlin, A., Mann, M., Patterson, B.D., Dreizler, A., Kliewer, C.J.: Development of two-beam femtosecond/picosecond one-dimensional rotational coherent anti-Stokes Raman spectroscopy. Time-resolved probing of flame wall interactions. Proc. Combust. Inst. **35**, 3723–3730 (2015)
8. Wichman, I.S., Bruneaux, G.: Head-on quenching of a premixed flame by a cold wall. Combust. Flame **103**, 296–310 (1995)
9. Popp, P., Baum, M.: Analysis of wall heat fluxes, reaction mechanisms, and unburnt hydrocarbons during the head-on quenching of a laminar methane flame. Combust. Flame **108**, 327–348 (1997)
10. Poinsot, T., Haworth, D., Bruneaux, G.: Direct simulation and modeling of flame-wall interaction for premixed turbulent combustion. Combust. Flame **95**, 118–132 (1993)
11. Lai, J., Chakraborty, N.: Effects of lewis number on head on quenching of turbulent premixed flames: a direct numerical simulation analysis. Flow Turbul. Combust. **96**(2), 279–308 (2015)
12. Popp, P., Smooke, M., Baum, M.: Heterogeneous/homogeneous reaction and transport coupling during flame-wall interaction. Symp. Int. Combust. Proc. **26**, 2693–2700 (1996)
13. Westbrook, C.K., Adamczyk, A.A., Lavoie, G.A.: A numerical study of laminar flame wall quenching. Combust. Flame **40**, 81–99 (1981)
14. Laget, O., Muller, L., Truffin, K., Kashdan, J., Kumar, R., Sotton, J., Boust, B., Bellenoue, M.: Experiments and modeling of flame/wall interaction in Spark-Ignition (SI) engine conditions SAE technical paper 2013-01-1121 (2013)
15. Boust, B., Sotton, J., Bellenoue, M.: Unsteady heat transfer during the turbulent combustion of a lean premixed methane–air flame: effect of pressure and gas dynamics. Proc. Combust. Inst. **31**, 1411–1418 (2007)
16. Boust, B., Sotton, J., Bellenoue, M.: Experimental study by high-speed particle image velocimetry of unsteady flame-wall inteaction in turbulent combustion. In: The International Symposia on Applications of Laser Techniques to Fluid Mechanics 13 (2006)
17. Bruneaux, G., Akselvoll, K., Poinsot, T., Ferziger, J.H.: Flame-wall interaction simulation in a turbulent channel flow. Combust. Flame **107**, 27–36 (1996)
18. Jainski, C., Lu, L., Sick, V., Dreizler, A.: Laser imaging investigation of transient heat transfer processes in turbulent nitrogen jets impinging on a heated wall. Int. J. Heat Mass Tran. **74**, 101–112 (2014)
19. Borghi, R., Casci, C.: On the structure and morphology of turbulent premixed flames. Recent Advances in the Aerospace Sciences, 117–138 (1985)
20. Slavinskaya, N.A., Frank, P.: A modelling study of aromatic soot precursors formation in laminar methane and ethene flames. Combust. Flame **156**, 1705–1722 (2009)
21. Poinsot, T., Veynante, D.: Theoretical and Numerical Combustion. Self-Publishing, Bordeaux, France (2012)
22. Renou, B., Boukhalfa, A.: An experimental study of freely propagating premixed flames at various lewis numbers. Combust. Sci. Technol. **162**, 347–370 (2001)
23. Kobayashi, H., Kawabata, Y., Maruta, K.: Experimental study on general correlation of turbulent burning velocity at high pressure. Symp. Int. Combust. Proc. **27**, 941–948 (1998)

24. Malm, H., Sparr, G., Hult, J., Kaminski, C.F.: Nonlinear diffusion filtering of images obtained by planar laser-induced fluorescence spectroscopy. J. Opt. Soc. Am. A **17**, 2148 (2000)
25. Perona, P., Malik, J.: Scale-space and edge detection using anisotropic diffusion. IEEE Trans. Pattern Anal. Machine Intell. **12**, 629–639 (1990)
26. Canny, J.: A computational approach to edge detection. IEEE Trans. Pattern Anal. Mach. Intell. **8**, 679–698 (1986)
27. Jainski, C., Rißmann, M., Böhm, B., Dreizler, A.: Experimental investigation of flame surface density and mean reaction rate during flame–wall interaction. Proc. Combust. Inst. (2016, in press)
28. Trouvé, A., Poinsot, T.: The evolution equation for the flame surface density in turbulent premixed combustion. J. Fluid Mech. **278**, 1–31 (1994)
29. Muppala, S.R., Aluri, N.K., Dinkelacker, F., Leipertz, A.: Development of an algebraic reaction rate closure for the numerical calculation of turbulent premixed methane, ethylene, and propane/air flames for pressures up to 1.0 MPa. Combust. Flame **140**, 257–266 (2005)
30. Peterson, B., Baum, E., Böhm, B., Dreizler, A.: Early flame propagation in a spark-ignition engine measured with quasi 4D-diagnostics. Proc. Combust. Inst. **35**, 3829–3837 (2015)